

Simulating quantum circuits using the multi-scale entanglement renormalization ansatz

I.A. Luchnikov,^{1,2} A.V. Berezutskii,^{1,2,3} and A.K. Fedorov^{1,2,4}

¹*Russian Quantum Center, Skolkovo, Moscow 143025, Russia*

²*Moscow Institute of Physics and Technology, Dolgoprudny, Moscow Region 141700, Russia*

³*Institut Quantique & Département de Physique,*

Université de Sherbrooke, Quebec J1K 2R1, Canada

⁴*Schaffhausen Institute of Technology, Geneva, Switzerland*

(Dated: December 30, 2021)

Understanding the limiting capabilities of classical methods in simulating complex quantum systems is of paramount importance for quantum technologies. Although many advanced approaches have been proposed and recently used to challenge quantum advantage experiments, novel efficient methods for approximate simulation of complex quantum systems are highly demanded. Here we propose a scalable technique for approximate simulations of intermediate-size quantum circuits on the basis of multi-scale entanglement renormalization ansatz (MERA). MERA is a tensor network, whose geometry together with orthogonality constraints imposed on its “elementary” tensors allows approximating many-body quantum states lying beyond the area-law scaling of the entanglement entropy. We benchmark the proposed technique for checkerboard-type intermediate-size quantum circuits of 27 qubits with various depths. Our approach paves a way to explore new efficient simulation techniques for quantum many-body systems.

I. INTRODUCTION

Recent progress in experiments with NISQ devices on demonstrating advantages in solving specific problems, such as random circuit sampling [1–3] and boson sampling [4–6], has stimulated a new wave of studies of fundamental limits of classical techniques in exact and approximate simulation of interacting many-body quantum systems. Specifically, various techniques utilizing matrix product state (MPS) [7, 8], projected entangled-pair states (PEPS) [9], neural network quantum states (NNQS) [10–12] have been used in simulating quantum circuits of dozens of qubits. New tensor network contraction techniques have been successfully used for the efficient simulation of the quantum supremacy circuits [13–15]. However, these still advanced methods suffer from many challenges. For example, MPS based simulators are restricted by the area-law scaling of the entanglement entropy. NNQS-based simulators suffer from inaccuracies induced by the noise coming from variational Monte Carlo (VMC) based calculations [16, 17]. The most advanced tensor network contraction algorithms for classical simulation of quantum supremacy circuits provides only measurement samples and does not provide the entire final state of a circuit.

One of the promising solutions of the problems listed above consists in building a simulator based on Multi-scale entanglement renormalization [18–20]. Multi-scale entanglement renormalization is a powerful numerical technique mostly used to analyze critical behavior of one-dimensional quantum systems. It utilizes a tensor network known as the multi-scale entanglement renormalization ansatz (MERA) to parametrize a many-body quantum state. In contrast with an MPS tensor network, which supports an area-law of entanglement entropy scaling in $1D$, i.e. $S_{\text{MPS}}(L) \sim \text{const}$, where L denotes system

size, MERA supports logarithmic entanglement entropy scaling with length of a $1D$ quantum many-body system, i.e. $S_{\text{MERA}} \sim \log(L)$ [21]. Since this logarithmic behavior of the entanglement entropy perfectly matches the scaling of the entanglement entropy of ground states of quantum critical systems [21, 22], MERA thus is a perfect tool for studying quantum criticality. Besides quantum criticality, the improved entanglement entropy scaling is a remarkable feature that can be exploited to build better classical simulator of quantum computations. In contrast to neural networks based approaches, MERA allows exact calculation of expectation values in most cases as well as MPS; therefore, MERA based simulator does not suffer from VMC induced noise. Meanwhile, MERA can describe many-body quantum states beyond the area law of entanglement entropy scaling as well as neural networks. Moreover, one can tune MERA by using efficient Riemannian optimization methods with preconditioning [23–25] (a.k.a. quantum natural gradient [26]). All this features make MERA a compromise solution in between MPS and NNQS that takes the best of both.

In this work, we propose and benchmark a MERA-based technique for approximate simulation of arbitrary quantum circuits. Within our technique, we fix the structure of the MERA and update “elementary” tensors of the MERA each time we apply a new quantum gate to the state parameterized by the MERA. Although this procedure is not always possible to do exactly, we can find the closest MERA to the exact circuit state. At each step, the update of the MERA tensors is implemented through maximization of the gate fidelity, which formulates a corresponding optimization problem with orthogonality constraints [27]. The significant simplification in this procedure comes from the fact that we update only blocks of the network that are not excluded because of the orthogonality constraints. We benchmark the pro-

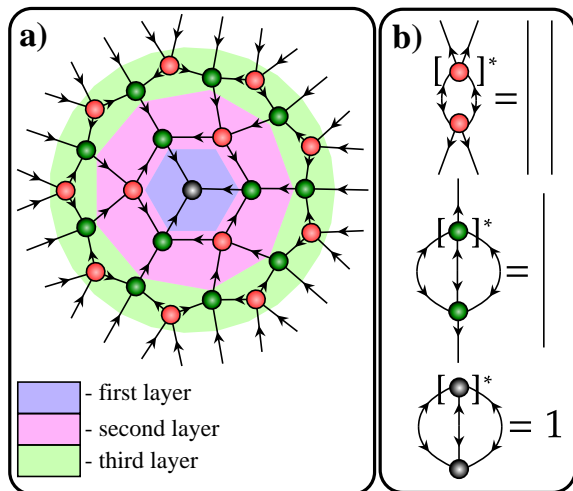


Figure 1: **a)** Diagrammatic representation of a three-layer ternary MERA tensor network: Red circles represent disentanglers and green circles stand for isometries. Arrows mark input and output edges of isometries and disentanglers. **b)** Diagrammatic representation of the isometries' and disentanglers' orthogonality property. Asterisk sign marks complex conjugation.

posed method for intermediate-size quantum circuits of 27 qubits with various depth.

Our work is organized as follows. In Sec. II, we provide a general description of the MERA architecture and the MERA-based quantum computations simulation protocol. In Sec. III, we present our simulation results of a random quantum circuit settings. We summarize our results and conclude in Sec. IV.

II. MERA-BASED SIMULATION OF QUANTUM COMPUTATIONS

To design a quantum computations simulation protocol, let us first discuss a MERA tensor network architecture in detail. We chose a basic ternary MERA architecture [20]. A three-layer ternary MERA is represented in Fig. 1 a) in terms of the graphical notation [28, 29]. The number of layers M defines the number of subsystems (qubits) $n = 3^M$, thus, the number of qubits in the ternary MERA represented in Fig. 1 a) is $n = 27$. Any MERA tensor network is combined from two types of elementary tensors, namely isometries and disentanglers. One can think of an isometry as the following linear isometric map:

$$\begin{aligned} v : \mathcal{H}_1^{\text{in}} \otimes \mathcal{H}_2^{\text{in}} \otimes \mathcal{H}_3^{\text{in}} &\rightarrow \mathcal{H}^{\text{out}}, \\ vv^\dagger &= I, \end{aligned} \quad (1)$$

where \dagger stands for the Hermitian conjugation, I is the identity operator, $\mathcal{H}_i^{\text{in}}$ is one of input Hilbert spaces and

\mathcal{H}^{out} is an output Hilbert space. The dimensions of those Hilbert spaces are connected as follows:

$$\dim(\mathcal{H}^{\text{out}}) = \begin{cases} \prod_{i=1}^3 \dim(\mathcal{H}_i^{\text{in}}), & \text{if } \prod_{i=1}^3 \dim(\mathcal{H}_i^{\text{in}}) \leq \chi, \\ \chi, & \text{otherwise,} \end{cases} \quad (2)$$

where χ is a hyper-parameter that defines the expressivity of a network (the ability of a network to represent highly-entangled quantum states) and the numerical complexity. Meanwhile, a disentangler is seen as a following unitary map

$$\begin{aligned} u : \mathcal{H}_1^{\text{in}} \otimes \mathcal{H}_2^{\text{in}} &\rightarrow \mathcal{H}_1^{\text{out}} \otimes \mathcal{H}_2^{\text{out}}, \\ u^\dagger u &= uu^\dagger = I, \end{aligned} \quad (3)$$

where the dimensions of input and output spaces are connected as follows:

$$\dim(\mathcal{H}_1^{\text{in}}) = \dim(\mathcal{H}_1^{\text{out}}), \quad (4)$$

$$\dim(\mathcal{H}_2^{\text{in}}) = \dim(\mathcal{H}_2^{\text{out}}). \quad (5)$$

Arrows in Fig. 1 depict the direction from input Hilbert spaces to output Hilbert space. The top layer of the MERA from Fig. 1 a) consists of only one tensor t that is also seen as the following isometric map

$$\begin{aligned} t : \mathcal{H}_1^{\text{in}} \otimes \mathcal{H}_2^{\text{in}} &\rightarrow \mathbb{C}, \\ t^\dagger t &= 1. \end{aligned} \quad (6)$$

The interpretation of the orthogonality property of elementary tensors in terms of the graphical notation is given in Fig. 1 b).

The orthogonality property of elementary tensors drastically reduces the numerical complexity of operations with MERA. To see this let us consider a calculation of a partial density matrix of two qubits. The full density matrix built upon the three-layer ternary MERA is given in Fig. 2 a). It is represented as two layers of tensor diagrams, i.e. the first layer represents $|\psi\rangle$ and the second layer represents $\langle\psi|$ in $\varrho = |\psi\rangle\langle\psi|$. To get a partial density matrix, we start to take traces over qubits that we want to exclude from consideration, i.e., we connect dangling edges of MERA and its complex conjugate version. Due to the orthogonality property one can introduce the reduction rules represented in Fig. 2 b). Applying these rules, we obtain the tensor network describing a partial density matrix whose diagrammatic representation is given in Fig. 2 c). One sees that this resulting tensor network is defined by only part of elementary tensors. The asymptotic contraction complexity of this network is about $O(\chi^8)M = O(\chi^8)\log(n)$ [20], which enjoys the *logarithmic scaling with the number of qubits*.

Let us turn to the design of the MERA-based simulation protocol for quantum circuits. Suppose one has a MERA tensor network that defines some many-qubit state $|\psi\rangle$. One needs to apply a two-qubit quantum gate to it, i.e., compute $U|\psi\rangle$. We do not consider the one-qubit case due to its simplicity – in this case, the gate can be simply merged into the tensor network, not breaking the isometry conditions. As for the two-qubit gates,

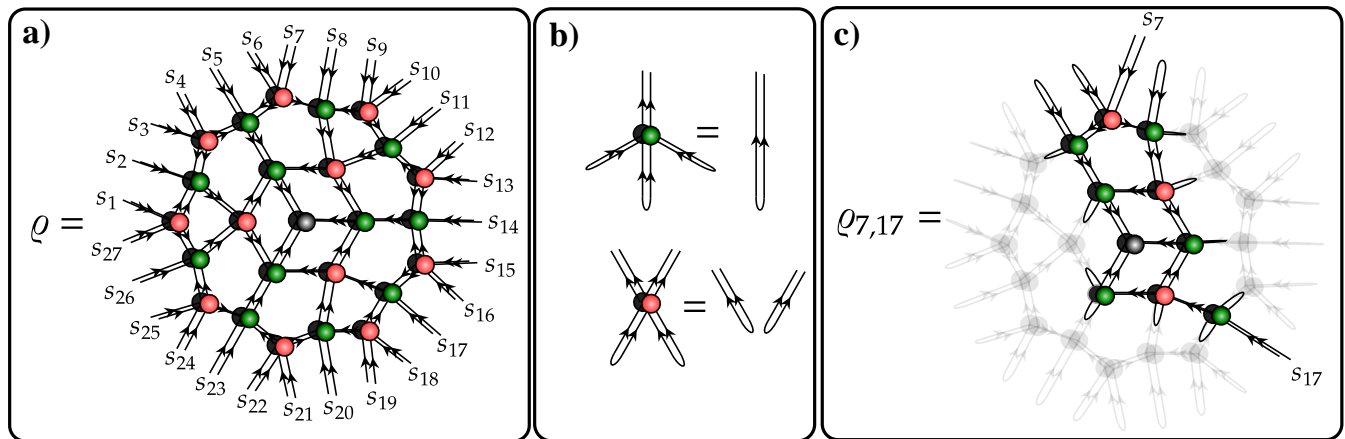


Figure 2: **a)** Diagrammatic representation of the density matrix built upon the MERA tensor network. Two layers correspond to $|\psi\rangle$ and $\langle\psi|$ in $\varrho = |\psi\rangle\langle\psi|$, s_i denotes i -th subsystem. **b)** Reduction rules based upon the orthogonality property. They drastically reduce the size of the resulting tensor network representing a partial density matrix. **c)** Partial density matrix of 7-th and 17-th subsystems. Loops connecting edges from different layers indicate a partial trace over a subsystem. Due to the orthogonality property only part of isometries and disentanglers contributes to the resulting density matrix.

one can simply absorb a two-qubit gate U into the entire MERA tensor network. However, this will change the topology of the tensor network and increase the complexity of all operations with the new tensor network. With adding more gates to the entire MERA network it quickly becomes numerically intractable. In contrast, we update the elementary tensors of the MERA in such a way that it represents the state after applying the gate U . In Fig. 3, we give diagrammatic interpretation of this idea. The updated version of MERA $|\psi'\rangle$ is of the same topology and the complexity of all operations remains the same. The updated version of MERA $|\psi'\rangle$ serves only as an approximation of $U|\psi\rangle$ due to the limited expressivity of a particular MERA architecture. To measure the accuracy of this approximation one can use the fidelity that reads

$$F(\psi, \psi') = |\langle\psi'|U|\psi\rangle|^2. \quad (7)$$

Due to the orthogonality property of elementary tensors, the calculation of the fidelity is greatly simplified if we update only those elementary tensors of the MERA which define the partial density matrix of two qubits connected with the gate U . We denote this subset of elementary tensors as $\mathcal{R}(U)$. Only these elementary tensors are depicted as updated tensors in Fig. 3. The diagrammatic representation of $\langle\psi'|U|\psi\rangle$ that defines the fidelity is given in Fig. 4. In order to get the best approximation $|\psi'\rangle$, one solves the following optimization problem:

$$\begin{aligned} & \underset{u, v \in \mathcal{R}(U)}{\text{maximize}} |\langle\psi'|U|\psi\rangle|^2, \\ & \text{subject to } uu^\dagger = I, \quad vv^\dagger = I. \end{aligned} \quad (8)$$

We solve this constrained optimization problem by using the preconditioned Riemannian ADAM optimizer on the

Protocol	Expressivity	Complexity
MPS-based	$\log(d)$	$O(d^3)$
MERA-based	$\log(n) \log(\chi)$	$O(\chi^8 \log(n))$

Table I: Theoretical comparison of MPS-based and MERA-based protocols for simulating quantum circuits.

complex Stiefel manifold [23, 30, 31]. This optimizer requires multiple calculations of the gradient of $|\langle\psi'|U|\psi\rangle|^2$ w.r.t the elementary tensors from $\mathcal{R}(U)$ and multiple calculations of preconditioners for all the elementary tensors from $\mathcal{R}(U)$ that are properly defined in Ref. [23]. To calculate both the gradient and preconditioners, we utilize the automatic differentiation technique [32]. The complexity of the automatic differentiation-based computation of the gradient and preconditioners is the same as the complexity of the fidelity computation [33, 34]. Therefore, under the assumption of the same number of optimization steps for any χ and n , the complexity of the overall optimization routine scales as the complexity of the density matrix calculation, i.e., as $O(\chi^8) \log(n)$, though with the large prefactor. For multiple quantum gates in a quantum circuit one needs to solve the optimization problem for each gate. Thus, using this MERA-based protocol, one can approximately simulate arbitrary quantum circuits.

Now let us compare the MPS-based quantum-computation simulation protocol with the proposed MERA-based protocol. We compare the two in terms of computational complexity and expressivity. We estimate the latter as an upper bound of the entanglement entropy supported by a particular protocol. This measure of expressivity is natural, because entanglement entropy can be thought of as a computational resource in

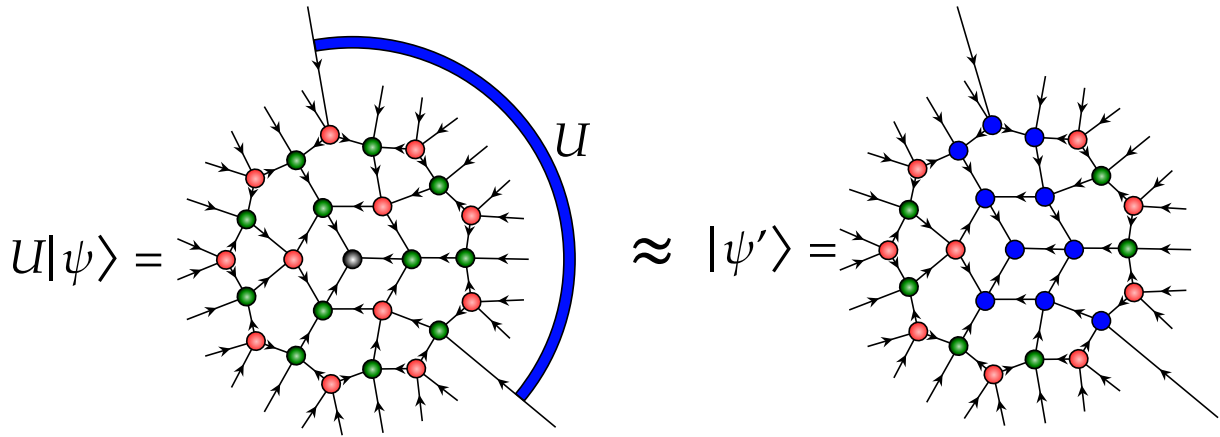


Figure 3: Transition from the MERA with a two-qubit gate to its approximation in terms of the single MERA with updated elementary tensors. Blue color marks the updated elementary tensors.

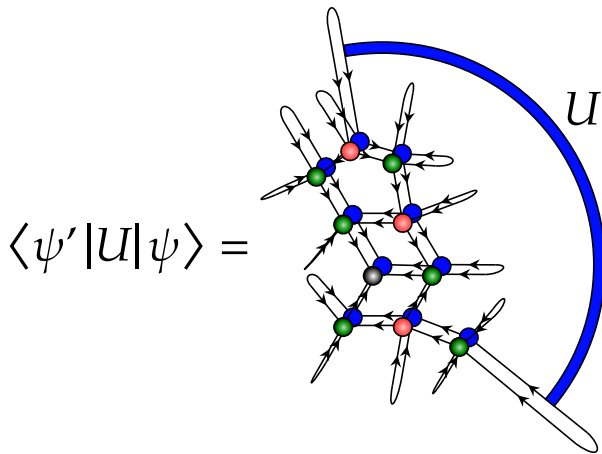


Figure 4: The diagrammatic representation of $\langle \psi' | U | \psi \rangle$ under the assumption that one updates only part of elementary tensors affecting the density matrix of qubits connected with U . The underlying layer of tensors is complex conjugated.

the paradigm of quantum computing. The expressivity of an MPS-based protocol scales as $\log(d)$, where d is the bond dimension of an MPS. The expressivity of MERA based protocol scales as $\log(n) \log(\chi)$. The complexity of a single gate update scales as $O(d^3)$ for an MPS-based protocol and as $O(\chi^8 \log(n))$ for the MERA based protocol. For better clarity, we organize these estimates in Table I.

One can see that if we increase the number of qubits in a system, the complexity and the expressivity of the MERA-based protocol increases logarithmically. Such a scaling is impossible for an MPS-based protocol since its complexity increases much faster than the expressivity in any scenario. Therefore, the MERA-based protocol is potentially more advantageous for systems consisting of a large number of qubits than MPS-based protocols. In the

next section we present numerical tests of the proposed protocol.

III. QUANTUM CIRCUITS SIMULATION NUMERICAL RESULTS

We validate the proposed simulation scheme by probing simulation of a randomly generated quantum circuit. This is a standard benchmark used to evaluate the performance of a particular simulation approach [8]. Gates in the circuit are placed in a checkerboard order as it is shown in Fig. 5. Each gate is generated randomly in two steps: 1) one samples real and imaginary parts of 4×4 matrix from the i.i.d normal distribution $\mathcal{N}(0, I)$, where I is the identity matrix; 2) one performs QR decomposition of the sampled matrix and utilizes unitary matrix Q as a two-qubit gate.

The initial state of the set of qubits is taken in the form $\bigotimes_{i=0}^{n-1} |\uparrow\rangle$, where \uparrow stands for the Bloch vector pointing to the north pole of the Bloch ball. In order to set the MERA tensor network to this initial state we solve the following optimization problem:

$$\begin{aligned} & \underset{u,v}{\text{maximize}} \sum_{i=1}^{n-1} |\langle \uparrow | \varrho_i | \uparrow \rangle|^2, \\ & \text{subject to } uu^\dagger = I, \quad vv^\dagger = I, \end{aligned} \quad (9)$$

where ϱ_i is i -th qubit's partial density matrix defined by the MERA tensor network. Having the MERA tensor network set in the initial state $\bigotimes_{i=0}^{n-1} |\uparrow\rangle$ one performs its elementary tensors' updates by solving the optimization problem Eq. (8) for each subsequent gate. After finishing all the updates one ends up with an approximation of the final quantum program's state in the form of MERA tensor network.

In order to evaluate the accuracy of the obtained ap-

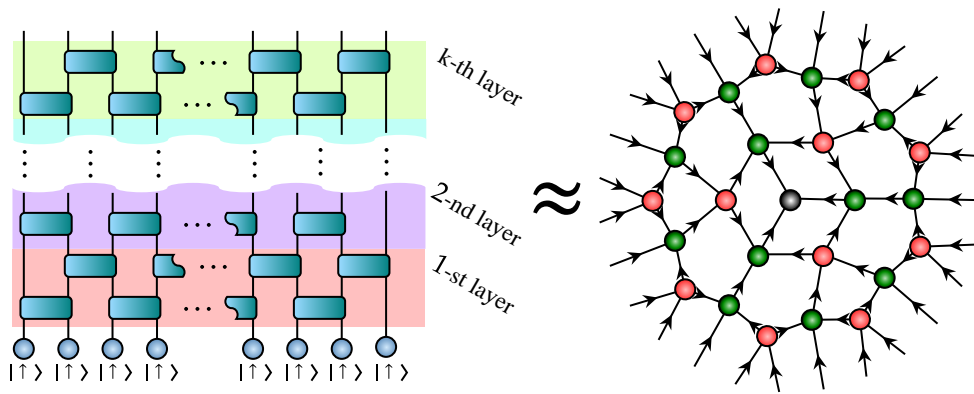


Figure 5: The left-hand side of the figure shows the tensor diagram of the checkerboard quantum program that is simulated via the proposed simulator. The right-hand side of the figure shows the MERA tensor network after nk updates (the entire quantum program) that is approximately equal to the final state of the program.

proximation, we calculate the following quantity:

$$\mathcal{F} = \prod_{i=1}^{nk} |\langle \psi_i | U_i | \psi_{i-1} \rangle|^2, \quad (10)$$

where k is the number of layers in the circuit that is also graphically defined in Fig. 5 and U_i is the i -th gate and $|\psi_i\rangle$ is the state represented by the MERA tensor network after i gates are applied. We note that the quantity in Eq. (10) comes for free, since i -th term in the product Eq. (10) is the optimal value of the objective function of the optimization problem Eq. (8) that is solved within i -th MERA update. In [8] it has been shown that \mathcal{F} is an accurate surrogate of the exact fidelity between the exact final state of a quantum program and an approximation. The value of \mathcal{F} ranges in the interval $[0, 1]$, and higher \mathcal{F} indicates a better approximation. The value of \mathcal{F} is equal to 1 iff the approximation is exact. One can also estimate an average fidelity of each two-qubit gate as follows

$$f \approx \mathcal{F}^{\frac{1}{nk}} \quad (11)$$

The value $\epsilon = 1 - f$ can be considered as the error rate per two-qubit gate, thus it serves as an interpretable measure of a NISQ device accuracy.

For the number of qubits $n = 27$ that corresponds to the three-layers MERA and χ ranging from 8 to 25, we have performed MERA-based simulation of random quantum circuit settings. We present \mathcal{F} as the function of the number of layers k in a quantum circuit and value of χ in Fig. 6.

As expected, the accuracy improves with the growth of χ , and deteriorates with the increase of the number of layers. The average fidelity of a two-qubit operation f for $\chi = 25$ is equal to 0.997 and the corresponding per-gate error rate is $\epsilon = 0.003$ that are comparable with the fidelity and error rate of a two-qubit operation of best real-world implementations of a quantum computing devices [1].

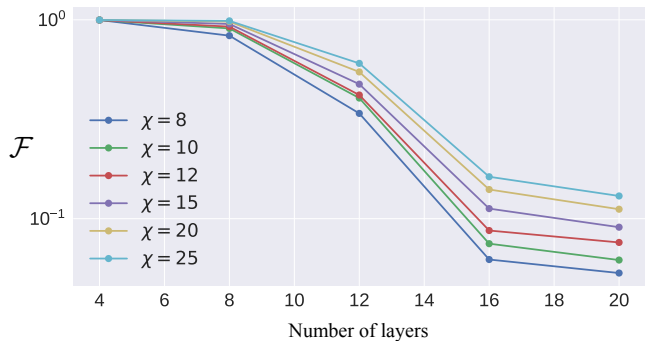


Figure 6: Fidelity estimation \mathcal{F} for checkerboard quantum circuits of different depths k for 27 qubits and various values of χ .

IV. DISCUSSION AND OUTLOOK

We have presented the protocol for the MERA-based classical simulation of arbitrary quantum circuits. We have demonstrated that our approach can be used for successful simulation of intermediate-size quantum circuits. Specifically, we have used random quantum circuits book-marking for 27-qubit checkerboard circuits. We have also discussed estimations showing that the MERA tends to outperform MPS based simulators for large n .

An essential next step is to perform this simulation for deeper MERA tensor networks and larger quantum circuits. It is also important to design an effective algorithm for sampling measurement outcomes from a MERA tensor networks in order to closer mimic the real quantum computational devices.

ACKNOWLEDGMENTS

The work was supported by the RSF Grant No. 19-71-10092 (Sec. II; analysis of the MERA ansatz), Lead-

ing Research Center on Quantum Computing (Agreement No. 014/20; Sec. III, development of the simulation method), and Russian Roadmap on Quantum Comput-

ing (experiments with intermediate-size circuits).

-
- [1] F. Arute, K. Arya, R. Babbush, D. Bacon, J. C. Bardin, R. Barends, R. Biswas, S. Boixo, F. G. Brandao, D. A. Buell, *et al.*, *Nature* **574**, 505 (2019).
- [2] Y. Wu, W.-S. Bao, S. Cao, F. Chen, M.-C. Chen, X. Chen, T.-H. Chung, H. Deng, Y. Du, D. Fan, *et al.*, *Physical review letters* **127**, 180501 (2021).
- [3] Q. Zhu, S. Cao, F. Chen, M.-C. Chen, X. Chen, T.-H. Chung, H. Deng, Y. Du, D. Fan, M. Gong, *et al.*, *Science Bulletin* (2021).
- [4] H.-S. Zhong, H. Wang, Y.-H. Deng, M.-C. Chen, L.-C. Peng, Y.-H. Luo, J. Qin, D. Wu, X. Ding, Y. Hu, *et al.*, *Science* **370**, 1460 (2020).
- [5] H. Wang, J. Qin, X. Ding, M.-C. Chen, S. Chen, X. You, Y.-M. He, X. Jiang, L. You, Z. Wang, *et al.*, *Physical review letters* **123**, 250503 (2019).
- [6] H.-S. Zhong, Y.-H. Deng, J. Qin, H. Wang, M.-C. Chen, L.-C. Peng, Y.-H. Luo, D. Wu, S.-Q. Gong, H. Su, *et al.*, *Physical review letters* **127**, 180502 (2021).
- [7] G. Vidal, *Physical review letters* **91**, 147902 (2003).
- [8] Y. Zhou, E. M. Stoudenmire, and X. Waintal, *Physical Review X* **10**, 041038 (2020).
- [9] C. Guo, Y. Liu, M. Xiong, S. Xue, X. Fu, A. Huang, X. Qiang, P. Xu, J. Liu, S. Zheng, *et al.*, *Physical review letters* **123**, 190501 (2019).
- [10] B. Jónsson, B. Bauer, and G. Carleo, arXiv preprint arXiv:1808.05232 (2018).
- [11] J. Carrasquilla, D. Luo, F. Pérez, A. Milsted, B. K. Clark, M. Volkovs, and L. Aolita, *Physical Review A* **104**, 032610 (2021).
- [12] G. Carleo, *Bulletin of the American Physical Society* (2021).
- [13] F. Pan and P. Zhang, arXiv preprint arXiv:2103.03074 (2021).
- [14] F. Pan, K. Chen, and P. Zhang, arXiv preprint arXiv:2111.03011 (2021).
- [15] J. Gray and S. Kourtis, *Quantum* **5**, 410 (2021).
- [16] G. Carleo and M. Troyer, *Science* **355**, 602 (2017).
- [17] G. Carleo, F. Becca, M. Schiró, and M. Fabrizio, *Scientific reports* **2**, 1 (2012).
- [18] G. Vidal, *Physical review letters* **99**, 220405 (2007).
- [19] G. Vidal, arXiv preprint arXiv:0912.1651 (2009).
- [20] G. Evenbly and G. Vidal, *Physical Review B* **79**, 144108 (2009).
- [21] G. Evenbly and G. Vidal, *Journal of Statistical Physics* **145**, 891 (2011).
- [22] G. Evenbly and G. Vidal, *Physical review letters* **102**, 180406 (2009).
- [23] M. Hauru, M. Van Damme, and J. Haegeman, *SciPost Phys* **10**, 040 (2021).
- [24] I. Luchnikov, M. Krechetov, and S. Filippov, *New Journal of Physics* (2021).
- [25] I. Luchnikov, A. Ryzhov, S. Filippov, and H. Ouerdane, *SciPost Physics* **10**, 079 (2021).
- [26] J. Stokes, J. Izaac, N. Killoran, and G. Carleo, *Quantum* **4**, 269 (2020).
- [27] A. Edelman, T. A. Arias, and S. T. Smith, *SIAM journal on Matrix Analysis and Applications* **20**, 303 (1998).
- [28] R. Orús, *Annals of Physics* **349**, 117 (2014).
- [29] J. C. Bridgeman and C. T. Chubb, *Journal of physics A: Mathematical and theoretical* **50**, 223001 (2017).
- [30] G. Bécigneul and O.-E. Ganea, arXiv preprint arXiv:1810.00760 (2018).
- [31] J. Li, L. Fuxin, and S. Todorovic, arXiv preprint arXiv:2002.01113 (2020).
- [32] H.-J. Liao, J.-G. Liu, L. Wang, and T. Xiang, *Physical Review X* **9**, 031041 (2019).
- [33] A. Griewank *et al.*, *Mathematical Programming: recent developments and applications* **6**, 83 (1989).
- [34] W. Baur and V. Strassen, *Theoretical computer science* **22**, 317 (1983).